



TITLE:

Dispersion of flexural waves in a borehole with a tensile fracture in an anisotropic stress environment

AUTHOR(S):

Kayama, Kosuke; Mikada, Hitoshi; Takekawa, Junichi

CITATION:

Kayama, Kosuke ...[et al]. Dispersion of flexural waves in a borehole with a tensile fracture in an anisotropic stress environment. *Geophysical Prospecting* 2021, 69(3): 598-607

ISSUE DATE:

2021-03

URL:

<http://hdl.handle.net/2433/276583>

RIGHT:

© 2021 The Authors. *Geophysical Prospecting* published by John Wiley & Sons Ltd on behalf of European Association of Geoscientists & Engineers.; This is an open access article under the terms of the Creative Commons Attribution-NonCommercial-NoDerivs License, which permits use and distribution in any medium, provided the original work is properly cited, the use is non-commercial and no modifications or adaptations are made.

Dispersion of flexural waves in a borehole with a tensile fracture in an anisotropic stress environment

Kosuke Kayama*, Hitoshi Mikada and Junichi Takekawa

Department of Civil and Earth Resources Engineering, Kyoto University, Kyoto, Japan

Received February 2020, revision accepted January 2021

ABSTRACT

The effect of tensile fracture in a vertical borehole under anisotropic horizontal stress conditions is numerically investigated in terms of the dispersion of flexural wave generated in dipole sonic logging. Our three-dimensional model comprises a borehole filled with water and a tensile fracture intersecting the borehole in the borehole axial direction. Two shear waves are excited individually to produce particle displacements polarized in two orthogonal radial directions using two dipole sources aligned in the two polarized directions. A vertical array of equispaced dipole sensors is placed at the centre of the borehole along the borehole axis. We assumed that the surrounding formation possesses transversally isotropic anisotropy with the isotropy plane parallel to the borehole axis due to horizontal stress anisotropy. We examined the dispersion of flexural waves travelling along a borehole in our numerical models that include either fast or slow formation with various depths of tensile fractures. Our numerical results show that the deeper the penetration depth of a tensile fracture, the higher the slowness of shear waves polarized perpendicular to the tensile fracture for both slow and fast formation models. Our results indicate that the flexural dispersion behaviour could be used to investigate the depth of penetration of a tensile fracture that can be produced by either drilling or hydraulic fracturing.

Key words: Anisotropy, Numerical study, Rock physics, Acoustics, Logging.

INTRODUCTION

Seismic waveforms are sensitive to properties and geometric shapes of materials in the wavepath, and their characteristics have been utilized in geophysical exploration. Sonic logging has been widely used as an effective method to obtain physical properties of formations surrounding the borehole. The usage of monopole and dipole sources enables us to estimate P- and S-wave velocities (Kitsunozaki, 1980) and even anisotropic properties could be estimated by use of cross-dipole sources orthogonally polarized towards the radial directions (Sinha and Kostek, 1996). Research on the dispersion of flexural waves travelling in the direction of borehole has

been of great interest since the application of logging tools with dipole sources. Sinha *et al.* (2009) investigated the effect of a steel pipe tool in a borehole on the dispersion curves and proved the influence of tools for the measurements. Sinha *et al.* (2010) have shown that the dispersion of flexural waves reflects the mechanical state of the surrounding material. Tang *et al.* (2016) studied elastic wave scattering due to the heterogeneities in the vicinity of the borehole. Fang *et al.* (2015) studied the effect of stress-induced anisotropy on the flexural dispersion. Wang and Fehler (2018a, b) investigated the influence of cement and casing pipe on the semblance and the dispersion curves. The above studies revealed that the physical properties, the inhomogeneities and the mechanical state of the materials surrounding the borehole have a significant influence on the dispersion of flexural waves.

*E-mail: kosuke.kayama@tansa.kumst.kyoto-u.ac.jp

During drilling or after hydraulic fracturing, tensile fracture along the borehole could be generated in the direction of principal stress orientation. As Maxwell (2014) mentioned, a microseismic observation system at hydraulic fracture treatments has proven invaluable to see the orientation and the dimension of artificially created fracture around the borehole. The distribution of acoustic emissions associated with hydraulic fracturing, however, may not directly indicate the fractured areas. Microseismic or acoustic emissions caused by drilling-induced tensile fractures generated at the time of drilling in fast formation could not be detected, either. Although the precise estimation of the penetration depth of induced tensile fractures has high demand, quantitative method for estimating the penetration depth of induced fractures has not been established yet. For evaluating the performance of hydraulic fracturing more precisely, an additional measurement of the penetration depth of induced fractures is desirable. Any fractures induced around borehole influence flexural wave propagation due to the induction of anisotropic elastic properties (Lei and Sinha, 2013), and the relationship between tensile fracture growth and flexural wave propagation has been pointed out (Zheng *et al.*, 2009; Su *et al.*, 2018). We hypothesize that the penetration depth of an induced fracture could be estimated by analysing the behaviour of flexural waves in the cross-dipole measurements in a quantitative manner.

In the present study, we investigate the influence of an induced tensile fracture in an anisotropic formation on flexural dispersion using numerical experiments. Since we may envisage fractures caused by hydraulic fracturing for both fast and slow formations, and drilling-induced fractures in the fast formation, numerical simulations in three-dimensional models comprised of a borehole and a lateral fracture filled with water intersecting the borehole both in fast and slow formations were carried out. The quantitative relationship between the penetration depth and dispersion characteristic of the flexural wave is investigated as a function of the depth of the fracture gradually varies in the range from 0 cm (i.e. without fracture) to infinity. We simulate seismic wave propagation in numerical models using the Hamiltonian particle method (HPM) with the staggered particles (Takekawa *et al.*, 2014a). The application of a modified matrix pencil algorithm (Ekstrom, 1995) to synthetic data sets produces the dispersion curves, which are investigated as a function of the depth of the tensile fracture. This may give us an opportunity to detect the fracture penetration depth through analysing the dispersion curves.

METHOD

In the present study, we use the Hamiltonian particle method (HPM) with the staggered particles (Takekawa *et al.*, 2014a) to simulate seismic wave propagation in three-dimensional numerical models. This method can simulate accurate seismic wavefield in models with irregularly shaped boundaries in an efficient manner (Takekawa *et al.*, 2014b). Finite-difference or finite-element method is often used to simulate seismic wave propagation. The finite-element method and its derivative ones like spectral element method have an advantage over the finite-difference method in the treatment of complex boundaries. However, the mesh generation process, which is a time-consuming task especially in three-dimensional cases, is required. On the other hand, HPM can simulate accurate seismic wavefield without such a time-consuming pre-process (Takekawa *et al.*, 2014b). Since our numerical model includes complex geometry (borehole and tensile fractures), we adopt the HPM as a seismic simulator. Derivation of particle motion equation of HPM can be found in the Appendix. One of the crucial factors to determine the numerical accuracy of HPM is the size of the influence domain. Takekawa *et al.* (2014b) investigated the effect of the influence domain on the numerical results and concluded that the compact support of the domain is better not only for the accuracy but also for the efficiency. We, therefore, set the radius of the influence domain to include only nearest neighbours.

In the present study, we need to model a borehole and lateral fractures which are filled by water. To represent fluid-filled borehole and fracture, we assign the physical properties of water to those particles corresponding to the borehole and fracture (Saenger *et al.*, 2004). In this case, a fracture is modelled as a tangential-stress-free rectangular plane whose physical properties are the same as water. The effect of the shape of the fracture tip on numerical accuracy depends on the spatial resolution. Takekawa *et al.* (2014c) investigated the influence of the spatial resolution on the accuracy of wavefield in cracked media using the HPM. They concluded that the numerical accuracy could be improved by increasing the spatial resolution around the fracture tip. According to the above study, we use sufficient spatial resolution for simulating an accurate seismic wavefield. We generated a synthetic data set using the HPM and then calculated the dispersion curves using the modified matrix pencil algorithm (Ekstrom, 1995). We compared the results from our method with the theoretical solutions and verified the accuracy of the HPM and the modified matrix pencil algorithm.

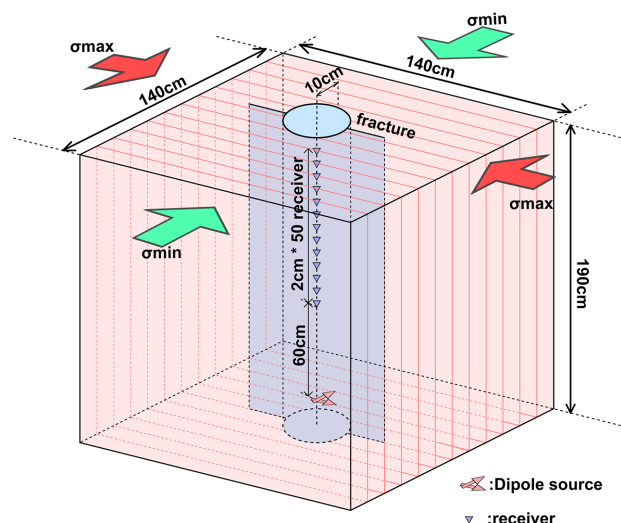


Figure 1 Schematic of the borehole model containing a tensile fracture.

NUMERICAL EXPERIMENT

Numerical model

Figure 1 shows a schematic of our numerical model. The model has a borehole and tensile fracture. In our numerical model, the fracture and its surrounding formation are represented in high resolution (2 mm), and large model size (7 * borehole radius) is required for simulating accurate flexural wave propagation especially in the low-frequency region. In order to reduce the computational cost, the receiver offset set up in the simulations is smaller than that of a real sonic logging tool. The change in receiver offset does not affect the extraction of the dispersion property of flexural waves because the geometry and physical properties are not changed along the borehole axis. We placed a cross-dipole source at the lower part of the model and plural receivers along the centre of the borehole axis with an interval of 2 cm. The receiver spacing is set denser than that in a real sonic logging tool to avoid spatial aliasing. These receivers record the particle velocity in the borehole radial direction. The diameter of the borehole is 20 cm. We assumed the width of the fracture changing from 2 to 4 mm with the depth varying in the range from 0 cm (i.e. without fracture) to infinity. In the infinite depth model, the tensile fracture reaches to the model edge, i.e. entirely separating the numerical model. The direction of the fracture plane is parallel to the maximum principal stress direction. We test two types of surrounding formations, i.e. fast and slow formations. The differential stress in the horizontal plane induces tensile fractures along the borehole and causes the azimuthal anisotropy

in seismic wave velocities as a function of the magnitude of the differential horizontal stress. In the present study, we assume that both the slow and fast formations exhibit 5% P-wave and S-wave velocity anisotropy induced by the crustal stress, as listed in Table 1 (Kimura *et al.*, 2016).

The source wavelet is a Ricker wavelet with 4 kHz centre frequency. The particle spacing and time steps are 2 mm and 0.000325 ms, respectively, in the numerical simulation. The total numbers of the iterations for the fast and slow formations are 10,000 and 15,000, respectively. We use the message passing interface parallel computing with four nodes for efficient calculations. An absorbing boundary condition (Cerjan *et al.*, 1985) is applied to suppress the artificial boundary reflection at the model edges.

Validation of the method

Takekawa *et al.* (2014b,c) investigated the numerical accuracy of the Hamiltonian particle method (HPM) for simulating the surface waves and wave propagation in cracked media. They investigated their method in the two-dimensional models and did not look into the applicability of the method to the propagation of flexural waves. It is, therefore, necessary to confirm the calculation accuracy of the HPM method for three-dimensional borehole models. We simulated flexural wave propagation in borehole without fractures in an isotropic formation model. In an isotropic formation model, full waveform and theoretical dispersion curve can be calculated by the semi-analytical approach noted in Tang and Cheng (2004). Figure 2 shows a comparison of shot gathers that are obtained from HPM and the discrete wavenumber integration method (Bouchon and Aki, 1977; Cheng and Toksöz, 1981) for a 4-kHz dipole source. The horizontal and vertical axes represent time and receiver offset, respectively. There is no visible difference between the waveforms, which indicates that the HPM can calculate seismic wavefield in a fluid-filled borehole with high accuracy. Figure 3 shows a comparison of the two dispersion curves, one for numerically simulated waveforms using HPM and the other theoretically predicted by the dispersion equation. Red circles represent numerical dispersion curves, and a cyan solid curve shows the theoretical dispersion curve. Both results have good agreement with each other, especially in the low-frequency range. In the fast formation model, the numerical result gradually deviates from the theoretical curve with increasing frequency. In the slow formation model, the slowness cannot be obtained by the modified matrix pencil algorithm for more than 8 kHz. Since it is difficult to calculate accurate seismic wavefield for high frequency component due

Table 1 Physical properties used in numerical experiments

	C11 (GPa)	C22 (GPa)	C12 (GPa)	C44 (GPa)	C55 (GPa)
Fluid	2.25	2.25	2.25	0.00	0.00
Fast formation	26.95	24.32	12.00	6.80	7.53
Slow formation	8.71	7.86	6.59	0.84	0.93

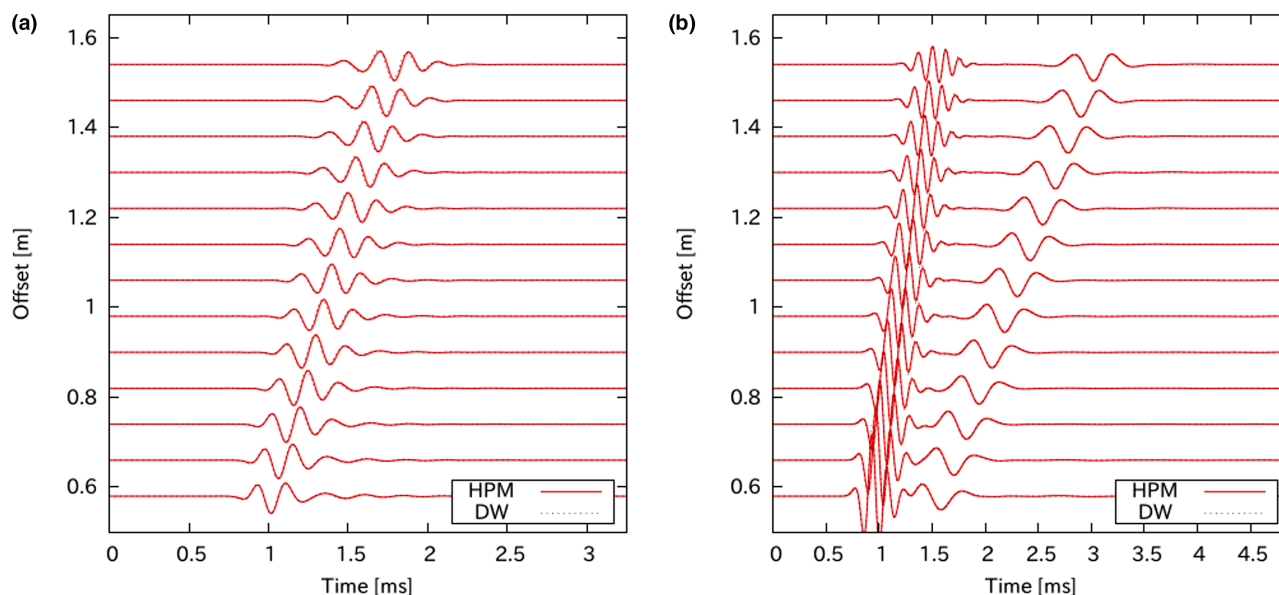


Figure 2 Comparison of shot gathers that are obtained from HPM (solid red lines) and discrete wavenumber integration method (dotted grey lines: overlapped with the red line) for (a) a fast formation and (b) a slow formation. The horizontal and vertical axes represent time and offset, respectively.

to the numerical dispersion, the error of the estimated slowness would be generated. Therefore, we restrict ourselves to use only around the peak frequency and do not use such high frequency ranges in this study. At 8 kHz, the errors of the slowness of the flexural wave between numerical and theoretical results are about 1.5% and 0.5% for the fast and slow formation models, respectively. We believe that our method can calculate the seismic wavefield and dispersion curves with sufficient accuracy. We could confirm the appropriateness of our numerical method quantitatively.

Simulation results

Figure 4 shows the snapshots of the numerical simulations in a cross-section parallel to the borehole axis using the fast and slow formation models. The fracture depth is set to 0 cm, i.e. without tensile fracture. In the fast formation, we can observe the refraction S-wave in the borehole, whereas the slow formation model does not generate the refraction S-wave because the S-wave velocity of the formation is slower than the P-wave

velocity of the inner fluid. In both models, the flexural wave propagating along the borehole can be observed.

Figure 5 shows shot gathers for the fast and slow formation models with 10 cm fracture depth. Red and blue lines represent recorded components parallel and perpendicular to the tensile fracture, respectively. In each figure, clear flexural waves can be identified. The difference in arrival time due to velocity anisotropy and tensile fracture is also observed. We apply the modified matrix pencil algorithm to the recorded waveforms in order to obtain the dispersion curves.

RESULTS AND DISCUSSION

At first, we investigate the effect of the fracture width on the dispersion curve. Figure 6 shows the dispersion curves of the fast and slow formation models with the fracture width of 2 and 4 mm. The penetration depth of the fracture is fixed to 10 cm. Red and blue symbols represent the dispersion curves obtained from the waveforms recorded in the directions parallel and perpendicular to the fracture plane, respectively. In

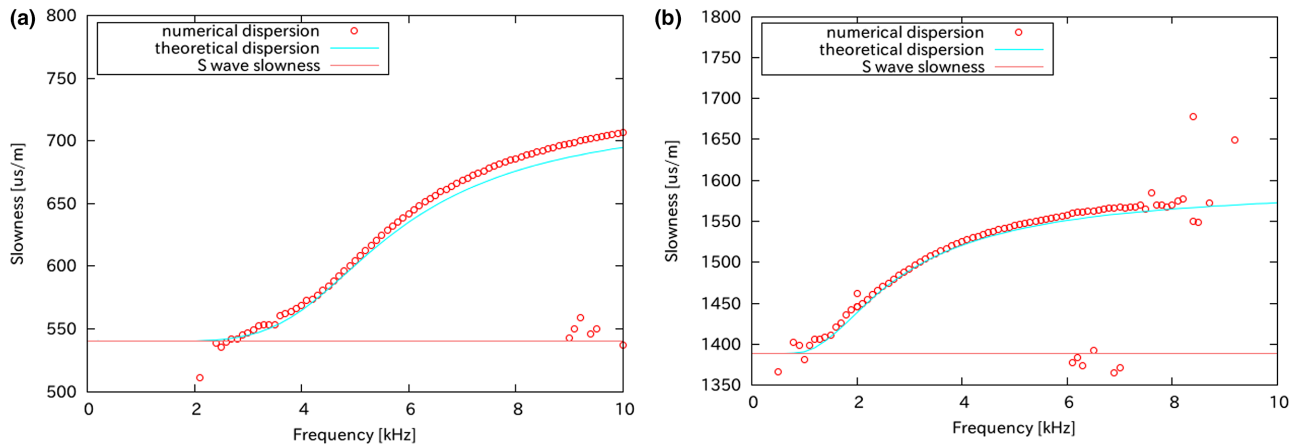


Figure 3 Comparison of numerical and theoretical dispersion curves for (a) a fast formation and (b) a slow formation. The horizontal and vertical axes represent frequency and slowness, respectively. Red circles and cyan solid curve represent numerical and theoretical curves, respectively. A horizontal straight red line depicts S-wave slowness of the surrounding formation.

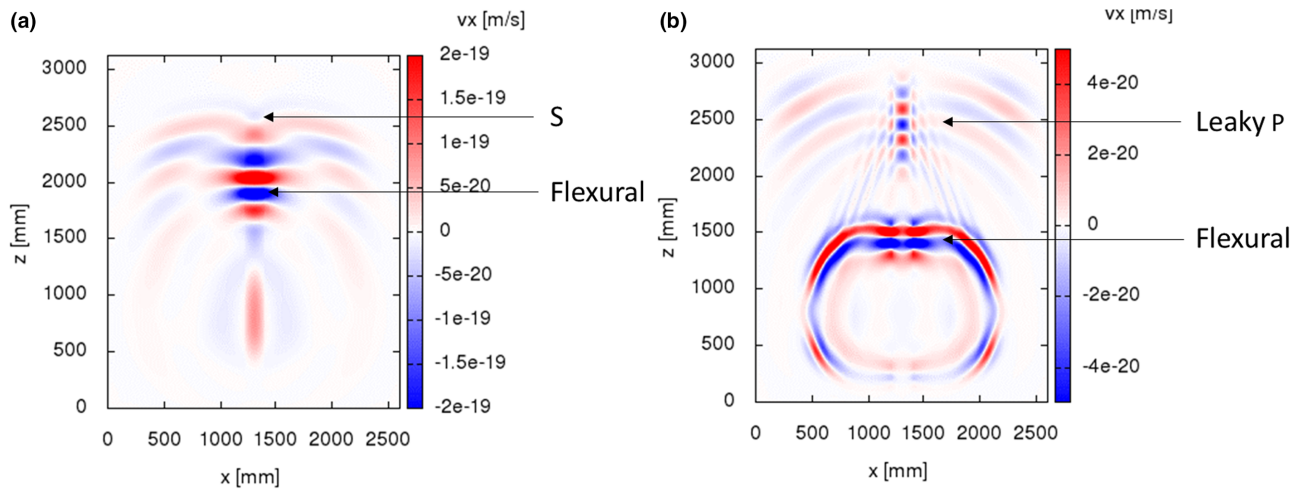


Figure 4 Two-dimensional cross-sectional snapshots of the wavefield for (a) a fast formation and (b) a slow formation. Contour colour represents the particle velocity in the x -direction.

the case of perpendicular direction (blue symbol), the dispersion curves obtained by both fracture width overlap with each other. On the other hand, for the case of parallel component, the clear difference between the 2 mm and 4 mm cases can be observed in both models. The results indicate that the parallel component is sensitive to the difference of fracture width whereas the dispersion curve obtained by the perpendicular component is not so much affected by the change of fracture width as that of the parallel component.

Next, we investigate the effect of fracture depth on the dispersion curve. Fracture width is fixed to 2 mm. Figure 7 shows the dispersion curves of the fast and slow formation models with the fracture depths of 0 cm and 10 cm. Red and

blue symbols represent dispersion curves in the directions of the parallel and perpendicular directions, respectively. Dispersion curves with different penetration depths in the parallel direction are nearly unchanged while those in the perpendicular direction show apparent change, especially in the low-frequency range. This result indicates that the perpendicular direction has the sensitivity to the fracture depth. Since our purpose is to evaluate the detectability of fracture growth (i.e. penetration depth of the fracture) by analysing the dispersion curve, we focus our attention on the perpendicular component in the following study.

We calculate the dispersion curves with various fracture depths, as shown in Figure 8. In high frequency range, the

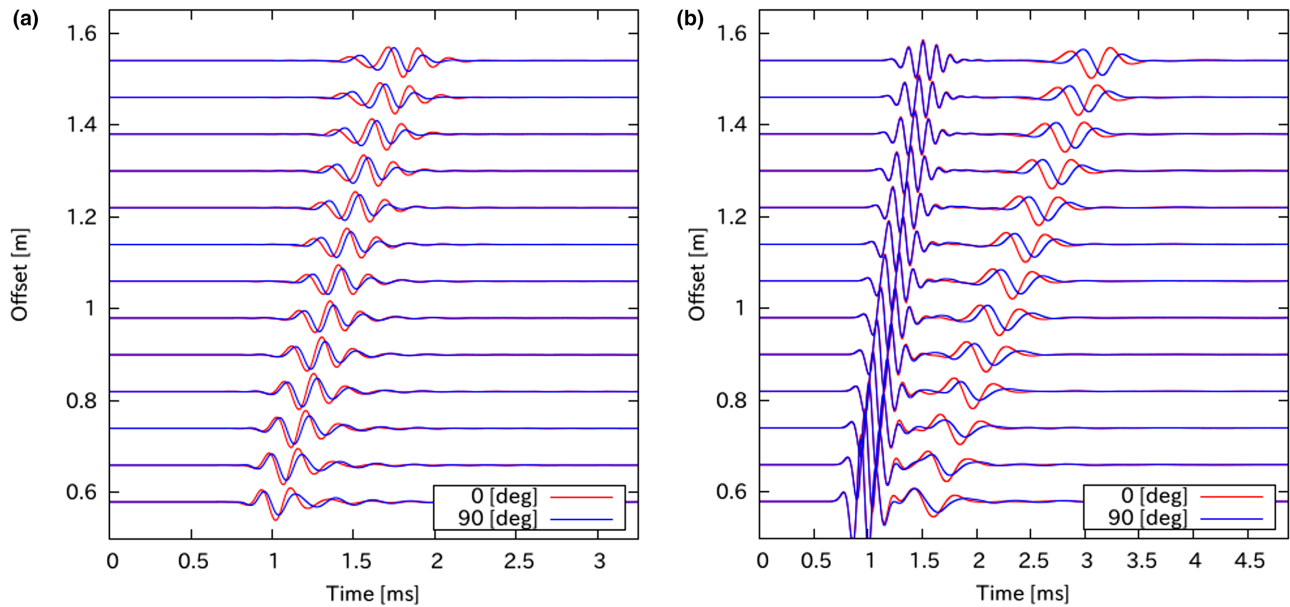


Figure 5 Shot gathers for (a) fast formation and (b) slow formation containing a 10-cm deep fracture. The horizontal and vertical axes represent time and offset, respectively. Red (0 [deg]) and blue (90 [deg]) waveforms, respectively, correspond to the data acquired in the directions parallel and perpendicular to the maximum horizontal stress direction.

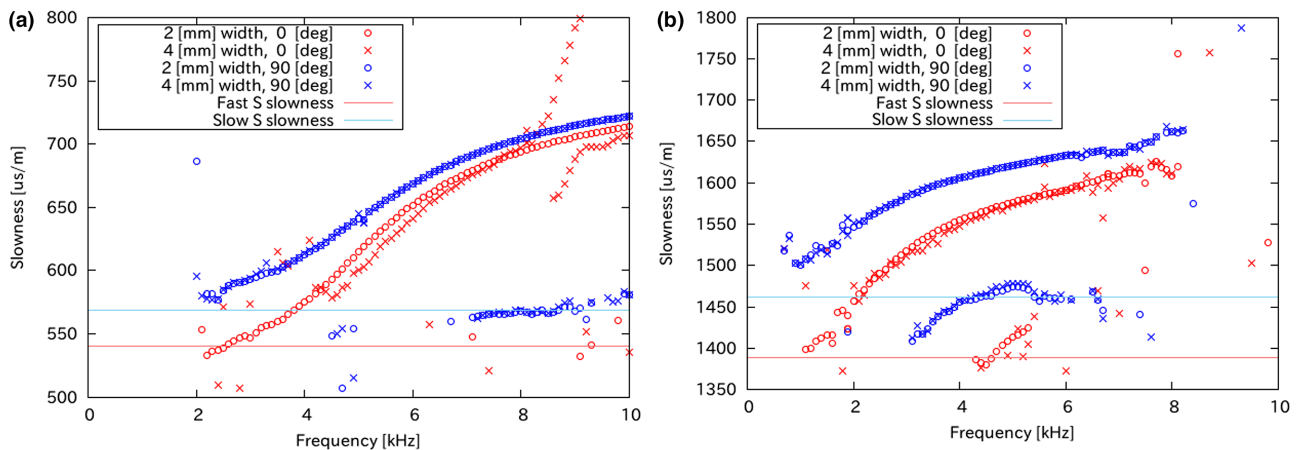


Figure 6 Dispersion curves for (a) fast formation and (b) slow formation containing fractures of different width. Red and blue symbols are the results of parallel and perpendicular components, respectively. Circles and crosses, respectively, represent the dispersion curves for fractures of 2 and 4 mm width. Red and blue lines are fast and slow S-wave slowness of the surrounding formation. The axes are the same as in Figure 3.

dispersion curves with each penetration depth are nearly identical. In low frequency range, on the other hand, each curve shows a clear distinction for both models. The deviations of the dispersion curves start around 7 and 4 kHz for fast and slow formation models. The wavelengths corresponding to these frequencies are almost the same as the diameter of the borehole, i.e. 20 cm. The relation of wavelength with the borehole diameter indicates that the size of the borehole primarily dominates the behaviour of the flexural wave in the high

frequency range, and, therefore, the dispersion curves in the frequency range lower than the frequencies of wavelengths of the borehole diameter would be sensitive to the penetration depth of the fracture. To investigate the effect of fracture depth on the estimated slowness, we focus the slowness in the low-frequency range, which is around the centre frequency of the source wavelet. The variations of the slowness at 4 kHz for the fast formation model and 3 kHz for the slow formation model with the fracture depths are depicted in Figure 9. The

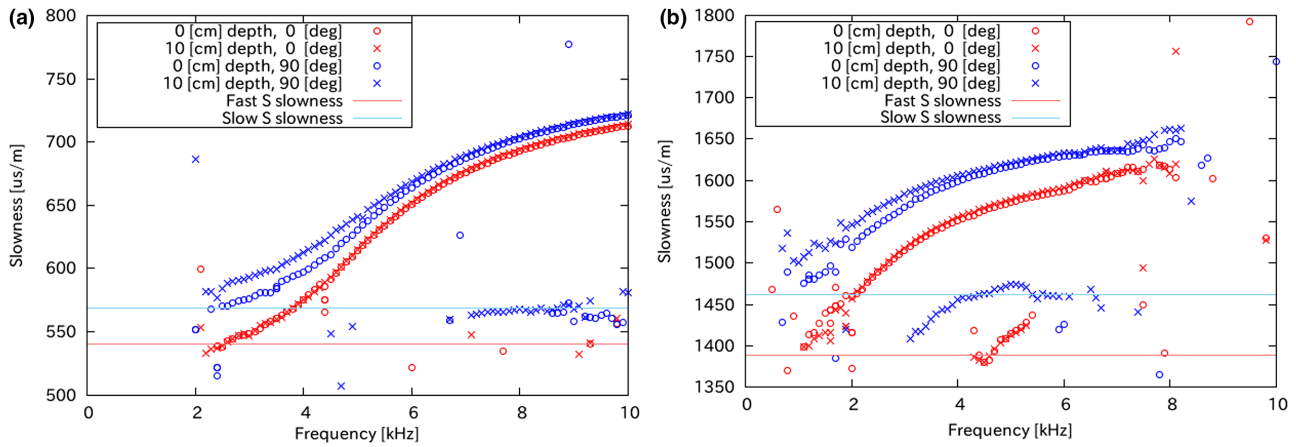


Figure 7 Dispersion curves for (a) fast formation and (b) slow formation containing fractures of different depth. Circles and crosses respectively represent the results for fractures of 0 and 10 cm depth. Other details are the same as in Figure 6.

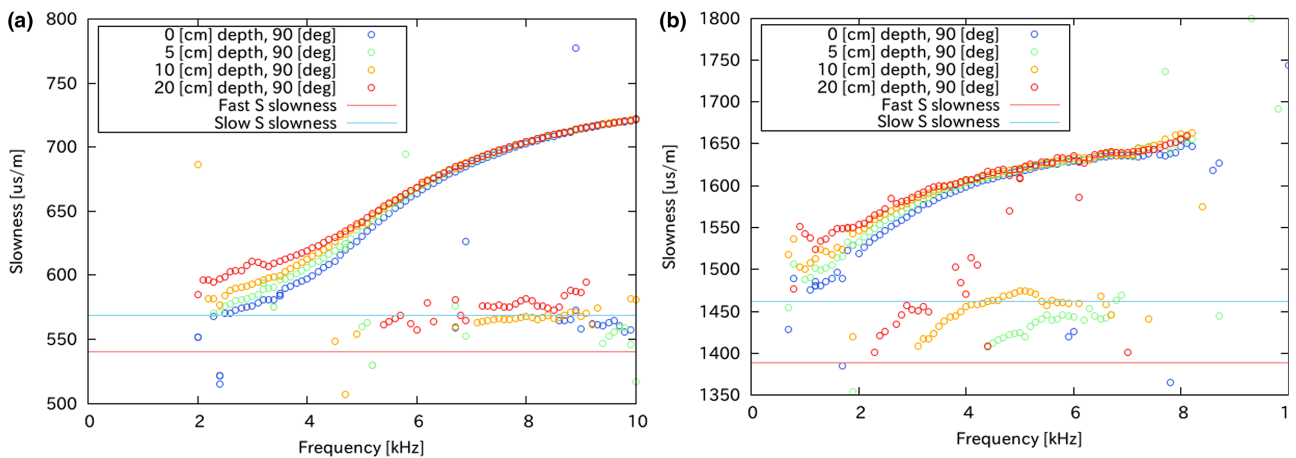


Figure 8 Dispersion curves of flexural waves polarized in the direction perpendicular to the fracture with fracture depth of 0 cm, 5 cm, 10 cm and 20 cm for (a) fast formation and (b) slow formation. Details are the same as in Figure 6.

horizontal and vertical axes are the fracture depth and the S-wave slowness, respectively. We can observe that the slowness increases with increasing the fracture depth and approaches the slowness of infinite depth case.

We show the change of the dispersion curves for both fast and slow formation models. In the dispersion curves in the direction perpendicular to the fracture plane, the estimated slowness monotonically increases as the fracture depth: S-wave slownesses increased by about 4.6% at 4 kHz in the fast, and about 1.2% at 3 kHz in the slow formations. The effect of tensile fracture appears more significant in the fast formation than in the slow formation. We observe in both models that the higher the slownesses, the deeper the fracture penetration. These results would indicate that the penetration depth of the lateral fracture is estimated in the analysis of the dispersion

curve of flexural waves polarized perpendicular to the fracture plane.

In the practice of hydraulic fracturing, the orientation and the dimension of artificially created fractures are monitored in microseismic monitoring, which may not directly indicate the zones of permeable fractures in the vicinity of the borehole. The present study would imply that time-lapse well logging to acquire the dispersion of flexural waves before and after the fracturing is a possible candidate to locate permeable fractures using the relation between the depth of artificially created tensile fractures and the change in S-wave slownesses in the vicinity of the borehole regardless of the formation to be fast or slow.

For accurate interpretation of the result of cross-dipole anisotropy measurements, estimating the penetrating depth of

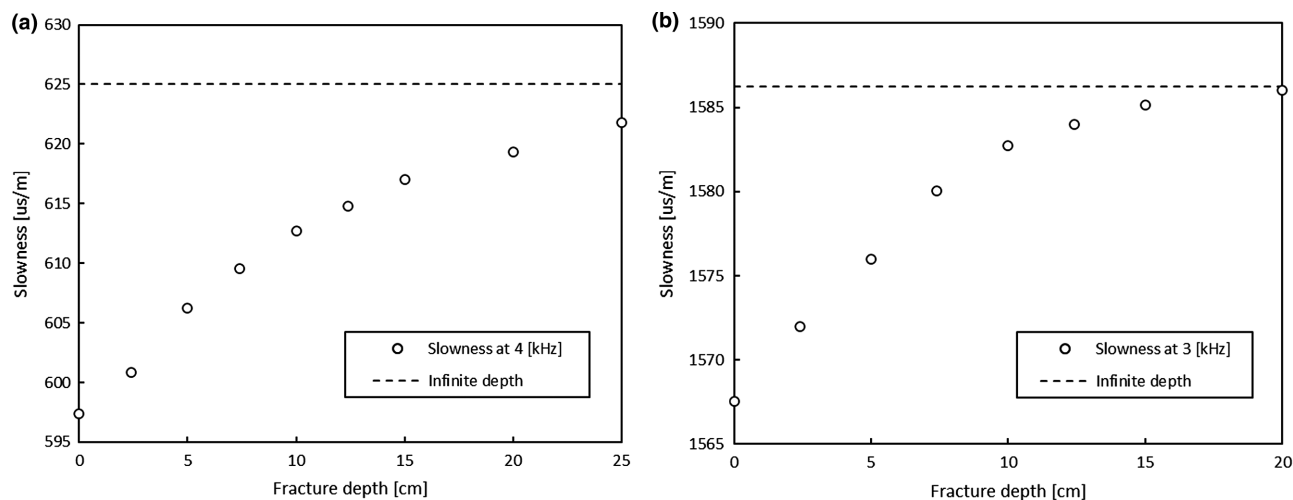


Figure 9 Slowness variations versus fracture depth for (a) fast formation at 4 kHz and (b) slow formation at 3 kHz. The dashed line represents the slowness of infinite fracture depth model.

induced fractures is one of the key factors (Zheng *et al.*, 2009). The implication of this study shows the possibility of more accurate interpretation of anisotropy of surrounding formations by combining the estimated penetration depth with rock physics models (Xu *et al.*, 2018).

CONCLUSIONS

We investigated the relationship between the penetration depth of the tensile fracture and the flexural dispersion in the borehole environment using numerical simulations. We first confirmed the validity of the numerical method through comparing the shot gathers and dispersion curves obtained from a semi-analytical approach and Hamiltonian particle method for an isotropic formation model without fracture. Our numerical results show good agreement with the shot gathers obtained from the discrete wavenumber integration method and the theoretical dispersion curves for fast and slow formation models. We then evaluated the variations of the dispersion curves with the penetration depth of the fracture. The slowness of flexural waves polarized perpendicular to the plane of fracture at low frequency monotonically and asymptotically increases with increasing fracture depth. The size of the borehole and the slowness of formation shear waves determine an appropriate frequency range for evaluating the penetration depth. The variation of the slowness of flexural waves is a function of the depth of the fracture. Therefore, this relation could be utilized to estimate fracture growth in hydraulic fracturing using cross-dipole measurement.


ACKNOWLEDGEMENTS


We appreciate Dr Angus Best, Dr Xinding Fang, the associate editor and two anonymous reviewers for their valuable comments and suggestions that improved our manuscript significantly. This work was supported by JSPS KAKENHI Grant Number 18K05012.

DATA AVAILABILITY STATEMENT

The data that support the findings of this study are available from the corresponding author upon reasonable request.

ORCID

Kosuke Kayama  <https://orcid.org/0000-0001-9441-4287>

Hitoshi Mikada  <https://orcid.org/0000-0002-9396-4209>

Junichi Takekawa  <https://orcid.org/0000-0003-2886-3425>

REFERENCES

- Bouchon, M. and Aki, K. (1977) Discrete wave-number representation of seismic-source wave fields. *Bulletin of the Seismological Society of America*, 67(2), 259–277.
- Cerjan, C., Kosloff, D., Kosloff, R., and Reshef, M. (1985) A nonreflecting boundary condition for discrete acoustic and elastic wave equations. *Geophysics*, 50, 705–708.
- Cheng, C.H. and Toksöz, M.N. (1981) Elastic wave propagation in a fluid-filled borehole and synthetic acoustic logs. *Geophysics*, 46(7), 1042–1053.

- Ekstrom, M.P. (1995) Dispersion estimation from borehole acoustic arrays using a modified matrix pencil algorithm. *Proceedings of the 29th Asilomar Conference on Signals, Systems and Computers*, 1, pp. 449–453.
- Fang, X., Cheng, A. and Fehler, M.C. (2015) Investigation of borehole cross-dipole flexural dispersion crossover through numerical modeling. *Geophysics*, 80(1), D75–D88.
- Kimura, T., Mikada, H., Araki, E., Kodaira, S. and Miura, S. (2016) Wide area distribution of S-wave anisotropy estimated by airgun surveys around seafloor cabled seismometers in the Nankai Trough, Japan. 86th SEG Annual Meeting, Dallas, U.S.A., Technical Program Expand Abstracts, 337–341.
- Kitsunezaki, C. (1980) A new method for shear-wave logging. *Geophysics*, 45(10), 1489–1506.
- Lei, T. and Sinha, B.K. (2013) Fracture-induced anisotropy and reflectivity of elastic waves in a fluid-filled borehole. 83rd SEG Annual Meeting, Houston, U.S.A., Technical Program Expand Abstracts, 504–508.
- Maxwell, S. (2014) *Microseismic Imaging of Hydraulic Fracturing*, Society of Exploration Geophysics.
- Saenger, E.H., Kruger, O.S. and Shapiro, S.A. (2004) Effective elastic properties of randomly fractured soils: 3D numerical experiments. *Geophysical Prospecting*, 52, 183–195.
- Sinha, B.K., Kane, M.R. and Frignet, B. (2010) Dipole dispersion crossover and sonic logs in a limestone reservoir. *Geophysics*, 65(2), 390–407.
- Sinha, B.K. and Kostek, S. (1996) Stress-induced azimuthal anisotropy in borehole flexural waves. *Geophysics*, 61(6), 1899–1907.
- Sinha, B.K., Simsek, E. and Asvadurov, S. (2009) Influence of a pipe tool on borehole modes. *Geophysics*, 74(3), E111–E123.
- Su, Y.D., Li, Z., Xu, S., Zhuang, C.X. and Tang, X.M. (2018) Elastic-wave evaluation of downhole hydraulic fracturing: Modeling and field applications. *Geophysics*, 83(1), D1–D8.
- Takekawa, J., Mikada, H. and Goto, T. (2014a) A Hamiltonian particle method with a staggered particle technique for simulating seismic wave propagation. *Pure and Applied Geophysics*, 171(8), 1747–1757.
- Takekawa, J., Mikada, H. and Goto, T. (2014b) An accuracy analysis of a Hamiltonian particle method with the staggered particles for seismic-wave modeling including surface topography. *Geophysics*, 79(4), T189–T197.
- Takekawa, J., Mikada, H. and Goto, T. (2014c) Numerical simulation using a Hamiltonian particle method for effective elastic properties in cracked media. *Exploration Geophysics*, 45(2), 116–124.
- Tang, X.M. and Cheng, A. (2004) Quantitative borehole acoustic methods. In: Helbig, K. and Treitel, S. (Eds.) *Handbook of Geophysical Exploration: Seismic Exploration*. Elsevier, pp. 31–72.
- Tang, X.M., Li, Z., Hei, C. and Su, Y.D. (2016) Elastic wave scattering to characterise heterogeneities in the borehole environment. *Geophysical Journal International*, 205, 594–603.
- Wang, H. and Fehler, M. (2018a) The wavefield of acoustic logging in a cased-hole with a single casing – Part I: A monopole tool. *Geophysical Journal International*, 212, 612–626.
- Wang, H. and Fehler, M. (2018b) The wavefield of acoustic logging in a cased-hole with a single casing – Part II: A dipole tool. *Geophysical Journal International*, 212, 1412–1428.

- Xu, S., Tang, X.M., Torres-Verdín, C. and Su, Y.D. (2018) Seismic Shear wave anisotropy in cracked rocks and an application to hydraulic fracturing. *Geophysical Research Letters*, 45(11), 5390–5397.
- Zheng, Y., Tang, X.M. and Patterson, D.J. (2009) Borehole acoustic dipole response with drilling-induced vertical fractures. 79th SEG Annual Meeting, Houston, U.S.A., Technical Program Expand Abstracts, 356–360.

APPENDIX

Hamiltonian particle method

This appendix briefly introduces the concept of the HPM method for calculating elastic wave field. In HPM, the error function e_i is defined as follows:

$$e_i = \sum_j \left\| \mathbf{F}_i \mathbf{r}_{ij}^0 - \mathbf{r}_{ij} \right\|^2. \quad (\text{A1})$$

where \mathbf{F} is the deformation gradient tensor, \mathbf{r}^0 and \mathbf{r} are the position vector at the initial and current time step, respectively. Subscripts i and j are indices for the target particle and its surrounding particles. \mathbf{r}_{ij} means the relative position vector between particles i and j . The deformation gradient tensor \mathbf{F} at position i is determined by minimizing the error function. The partial derivative of e_i with respect to \mathbf{F}_i is as follows:

$$\begin{aligned} \frac{\partial e_i}{\partial \mathbf{F}_i} &= 2 \sum_j \left(\mathbf{F}_i \mathbf{r}_{ij}^0 - \mathbf{r}_{ij} \right) \otimes \mathbf{r}_{ij}^0 \\ &= 2 \left(\sum_j \mathbf{F}_i \mathbf{r}_{ij}^0 \otimes \mathbf{r}_{ij}^0 - \sum_j \mathbf{r}_{ij} \otimes \mathbf{r}_{ij}^0 \right) \\ &= 2 \left(\mathbf{F}_i \sum_j \mathbf{r}_{ij}^0 \otimes \mathbf{r}_{ij}^0 - \sum_j \mathbf{r}_{ij} \otimes \mathbf{r}_{ij}^0 \right), \end{aligned} \quad (\text{A2})$$

where \otimes means the tensor product. The deformation gradient tensor can be obtained by setting the above equation to zero.

$$\begin{aligned} \mathbf{F}_i \sum_j \mathbf{r}_{ij}^0 \otimes \mathbf{r}_{ij}^0 - \sum_j \mathbf{r}_{ij} \otimes \mathbf{r}_{ij}^0 &= \mathbf{0}. \\ \mathbf{F}_i &= \left(\sum_j \mathbf{r}_{ij} \otimes \mathbf{r}_{ij}^0 \right) \mathbf{A}_i^{-1}. \\ \mathbf{A}_i &= \sum_j \mathbf{r}_{ij}^0 \otimes \mathbf{r}_{ij}^0. \end{aligned} \quad (\text{A3})$$

The strain energy V can be defined by using the stress and strain tensors.

$$V = \sum_i (\mathbf{E}_i : \mathbf{S}_i \Delta B_i) / 2. \quad (\text{A4})$$

where ΔB_i is the volume of particle i , \mathbf{S}_i is the stress tensor, \mathbf{E}_i is the strain tensor which can be calculated by the deformation gradient tensor. The total energy of the system defines the Hamiltonian H .

$$H = V + \sum_i m_i \|\mathbf{v}_i\|^2 / 2. \quad (\text{A5})$$

where m_i and \mathbf{v}_i are the mass and velocity of particle i . The equation of motion for each particle is obtained as follows:

$$m_i \frac{\partial \mathbf{v}_i}{\partial t} = \sum_i \mathbf{F}_i \mathbf{S}_i \mathbf{A}_i^{-1} \mathbf{r}_{ij}^0 \Delta B_i. \quad (\text{A6})$$

We apply a symplectic scheme to update position vectors of each particle. Details of the method can be found in the literature (Takekawa *et al.*, 2014a).